Unconventional Superconductivity in the BiS_2-Based Layered Superconductor $NdO_{0.71}F_{0.29}BiS_2$

Yuichi Ota,[1] Kozo Okazaki,[1,*] Haruyoshi Q. Yamamoto,[1] Takashi Yamamoto,[1] Shuntaro Watanabe,[2] Chuangtian Chen,[3] Masanori Nagao,[4,5] Satoshi Watauchi,[4] Isao Tanaka,[4] Yoshihiko Takano,[5,6] and Shik Shin[1,†]

[1]*Institute for Solid State Physics (ISSP), University of Tokyo, Kashiwa, Chiba 277-8581, Japan*
[2]*Research Institute for Science and Technology, Tokyo University of Science, Chiba 278-8510, Japan*
[3]*Beijing Center for Crystal R&D, Chinese Academy of Science (CAS), Zhongguancun, Beijing 100190, China*
[4]*Center for Crystal Science and Technology, University of Yamanashi, Kofu 400-8511, Japan*
[5]*National Institute for Materials Science, Tsukuba, Ibaraki 305-0047, Japan*
[6]*University of Tsukuba, Graduate School of Pure and Applied Sciences, Tsukuba, Ibaraki 305-8577, Japan*

(Received 11 October 2016; revised manuscript received 11 January 2017; published 17 April 2017)

We investigate the superconducting-gap anisotropy in one of the recently discovered BiS_2-based superconductors, $NdO_{0.71}F_{0.29}BiS_2$ ($T_c \sim 5$ K), using laser-based angle-resolved photoemission spectroscopy. Whereas the previously discovered high-T_c superconductors such as copper oxides and iron-based superconductors, which are believed to have unconventional superconducting mechanisms, have $3d$ electrons in their conduction bands, the conduction band of BiS_2-based superconductors mainly consists of Bi $6p$ electrons, and, hence, the conventional superconducting mechanism might be expected. Contrary to this expectation, we observe a strongly anisotropic superconducting gap. This result strongly suggests that the pairing mechanism for $NdO_{0.71}F_{0.29}BiS_2$ is an unconventional one and we attribute the observed anisotropy to competitive or cooperative multiple paring interactions.

DOI: 10.1103/PhysRevLett.118.167002

Since the discovery of the BiS_2-based superconductor $LaO_{1-x}F_xBiS_2$ by Mizuguchi *et al.* [1], this class of superconductors has attracted much attention and several new members were found soon after that [2–6]. They have several features similar to those of the previously discovered high-T_c superconductors of copper oxides (cuprates) [7] and iron-based superconductors [8]; that is, they have a layered crystal structure, and in $LnO_{1-x}F_xBiS_2$ (Ln = lanthanoid) superconductivity emerges at various Ln contents [9] with electron doping caused by the substitution of F for O like the iron pnictide $LnFeAsO_{1-x}F_x$ (1111 system). Hence, the mechanism of superconductivity in BiS_2-based superconductors may be expected to resemble that of the iron pnictides. However, in contrast to the other high-T_c superconductors, the conduction bands of BiS_2-based superconductors consist mainly of Bi $6p$ electrons [10], which are expected to have relatively weak electronic correlations, rather than $3d$ electrons, which have strong correlations that have been considered as indispensable for high-T_c superconductivity. Hence, in BiS_2-based superconductors, conventional electron-phonon coupling might be considered to be dominant for their superconductivity.

However, recent neutron scattering experiments have indicated that the electron-phonon coupling is much weaker than expected from the above scenario [11] and suggested the importance of charge fluctuations to superconductivity in BiS_2-based superconductors [12]. In addition, a large $2\Delta/k_BT_c$ suggests that the pairing mechanism is unconventional [13,14], and theoretical studies have suggested unconventional superconducting (SC) pairing mechanisms on the basis of calculations that assume superconductivity driven purely by electron-electron coupling [10,15–18]. These studies have indicated that the Fermi surface (FS) topology and SC gap anisotropy depend strongly on carrier doping; hence, it is crucial for understanding the superconducting mechanism to directly observe the band structure and SC gap anisotropy in these compounds.

Angle-resolved photoemission spectroscopy (ARPES) is a powerful tool for direct observation of the electronic structure and SC gap [19], and it has already been used to reveal the basic electronic structure of BiS_2-based superconductors [20,21]. For $NdO_{1-x}F_xBiS_2$, which has a maximum T_c of 5.6 K [4], FSs smaller than those expected from the nominal doping have been reported [20,21]. Direct observation of the SC gap in low-T_c materials with T_c as low as ~ 3 K has recently become possible by using a laser-ARPES apparatus that achieves the maximum energy resolution of 70 μeV and the lowest temperature of 1.5 K. Using this apparatus, we measured the band structure and SC gap anisotropy of a 29% F-doped sample ($NdO_{0.71}F_{0.29}BiS_2$, $T_c \sim 5$ K) and found highly anisotropic SC gaps. By carefully adjusting the focal point of the laser and reducing the spot size to as small as $\sim$100 μm at the cleaved sample surface, we can probe a region of few defects and detect a highly anisotropic and possibly nodal SC gap structure. We conclude that our result strongly suggests that $NdO_{0.71}F_{0.29}BiS_2$ is an unconventional superconductor that has competitive or cooperative multiple pairing interactions.

High-quality single crystals of $NdO_{0.71}F_{0.29}BiS_2$ were grown by a CsCl/KCl flux as described in Ref. [22].

The amount of F substitution for O was determined from electron probe microanalysis measurements. Clean surfaces were obtained by cleaving the sample *in situ* under ultrahigh vacuum (better than 5×10^{-11} Torr). ARPES measurements were performed using the He Iα ($h\nu = 21.218$ eV) resonance line with a VG-Scienta R4000 electron analyzer and using a vacuum ultraviolet (VUV) laser ($h\nu = 6.994$ eV) with a VG-Scienta HR8000 electron analyzer [23]. To minimize the space charge effect, the repetition rate of the VUV laser was raised to 960 MHz. The average power of the VUV laser is on the order of 10 μW and does not affect the cleanliness of the sample surfaces. The total energy resolution was set to 15 meV for the measurements using the He discharge lamp and to ~1.2 and 4 meV for the SC gap measurements and FS and $E - k$ map measurements, respectively, using the VUV laser. More details of the laser ARPES apparatus have been described in the literature [23–25]. The SC transition temperature was confirmed by magnetization measurements before the ARPES measurements of the same samples.

First, we determined the FS topology and the positions of the Fermi momentum (k_F) for all the FSs. Figures 1(a) and 1(c) show the FS maps measured using the He Iα line at 10 K and using a VUV laser with circular (c) polarization at 8 K, respectively, and Fig. 1(d) is the enlarged plot of the region indicated by the solid square in Fig. 1(c). The k_F positions of the FSs were determined by fitting the momentum distribution curves (MDCs) to Lorentzians and are indicated by the symbols on the FS maps in Figs. 1(a), 1(c), and 1(d). The FS maps were created from the MDCs integrated within ± 5 meV of E_F. Figures 1(b) and 1(e) show the E-k maps measured using the He Iα line and the VUV laser along cuts 1 and 2 shown in Figs. 1(a) and 1(c), respectively. The E-k map in Fig. 1(b) clearly shows that the FSs are composed of an electronlike band, whereas that in Fig. 1(e) shows that two electron bands are separated along this momentum cut [26]. Two FSs are recognized in this region, as indicated by the red and blue symbols in Figs. 1(c) and 1(d), and we call these FS sheets the outer and inner FSs, respectively. However, in the region indicated by the green symbols, two FS sheets are almost degenerate and cannot be separated. We call this region the degenerate region. The outer and inner FSs enclose 6.3% and 5.0% of the Brillouin zone area, respectively, and this corresponds to electron doping of 22.6% per Bi site. This is almost consistent with the electron doping expected from the amount of F substitution determined from electron probe microanalysis, and in contrast to the observation that the FS volume was considerably smaller than that expected from the nominal amount of F substitution for $NdO_{0.7}F_{0.3}BiS_2$ by Zeng *et al.* [21] This may be attributable to the better quality of our samples or bulk sensitivity of our measurements. Additionally, the shape of the FSs differs somewhat from that previously observed, and it is winding in the degenerate region and curved in the separation region. This should also

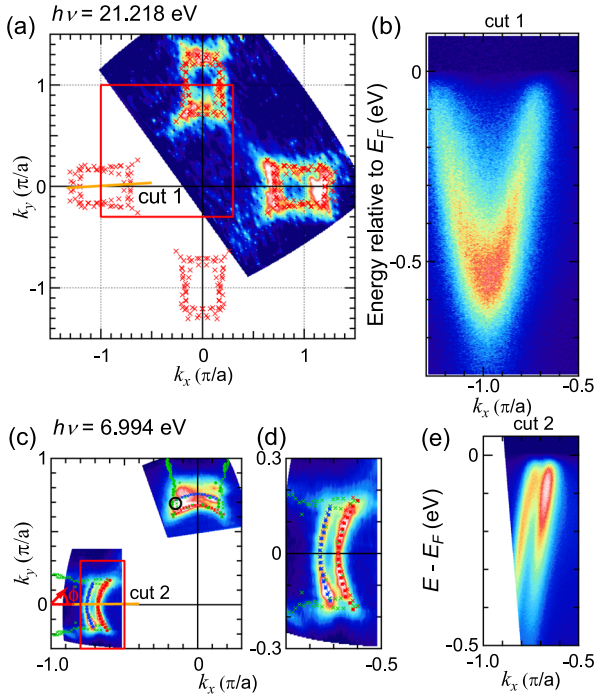

FIG. 1. FS and E-k maps of $NdO_{0.71}F_{0.29}BiS_2$. FS maps measured using (a) He Iα at 10 K and (c) a VUV laser at 8 K. The integration energy window of each FS map is ± 5 meV from E_F. Red, blue, and green symbols indicate the positions of k_F. The solid square in (a) corresponds to the region displayed in (c). The definition of the FS angle ϕ is shown in (c), and the open circle in (c) indicates the k_F for the temperature-dependent EDC shown in Fig. 2(a). (b) E-k map along cut 1 in (a) measured using He Iα at 10 K. (d) Enlarged plot for the region indicated by the solid square displayed in (c). (e) E-k map along cut 2 in (c) measured using the VUV laser at 8 K.

be originated from the fact that the amount of F substitution for our samples is larger than that for the samples measured by Zeng *et al.*

Next, to reveal the SC gap structure of $NdO_{0.71}F_{0.29}BiS_2$, we measured the SC gaps on the two electron FS sheets using the VUV laser. The energy distribution curves (EDCs) symmetrized with respect to E_F are shown in Fig. 2 [27]. Figure 2(a) shows the temperature-dependent symmetrized EDCs at k_F indicated by the open circle in Fig. 1(c). A valley structure at E_F indicates the existence of the SC gap, and it vanishes at a temperature close to T_c within a narrow temperature range (4.9–5.1 K) reflecting a clear transition between the normal and superconducting phases. We quantified the SC gap size by fitting the EDCs to the Bardeen-Cooper-Schrieffer (BCS) spectral function as shown in Fig. S2 of the Supplemental Material [28], and the deduced temperature-dependent SC gap size $\Delta(T)$ is shown in Fig. 2(b). More detailed analyses to ensure the validity of our evaluation of the SC gap size are described in Supplemental Material [28]. The solid line indicates the temperature dependence of the SC gap size based on the BCS theory for $\Delta(0) = 810$ μeV and $T_c = 5$ K, corresponding to

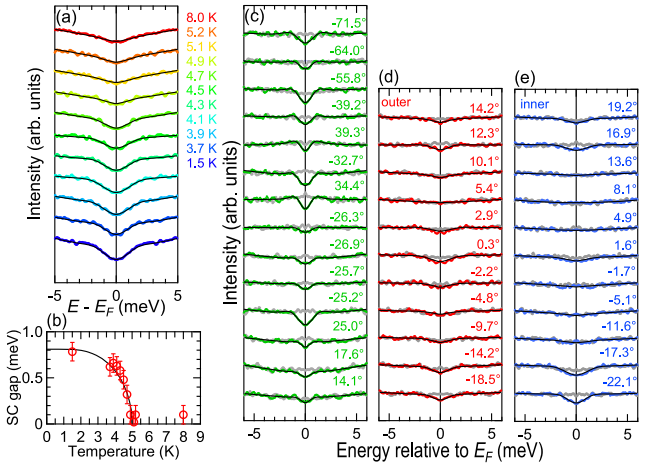

FIG. 2. Temperature-and FS-angle-dependent symmetrized EDCs at k_F measured using c-polarized light. (a) Temperature-dependent EDC symmetrized with respect to E_F at k_F indicated by the open circle in Fig. 1(c). (b) Temperature dependence of the SC gap size deduced from the fitting. The solid line indicates the SC gap size from the BCS theory for $\Delta(0) = 810$ μeV and $T_c = 5$ K. (c)–(e) Symmetrized EDCs at k_F (c) in the degenerate region, and clearly separated region of (d) outer FS and (e) inner FS. The EDCs were measured at 1.5 and 8 K ($T_c \sim 5$ K) for various FS angles ϕ, as shown in each panel. Gray symbols indicate the EDCs above T_c, and solid lines indicate the fitting functions using a BCS spectral function. EDCs before symmetrization are shown in Fig. S2 of Supplemental Material [28].

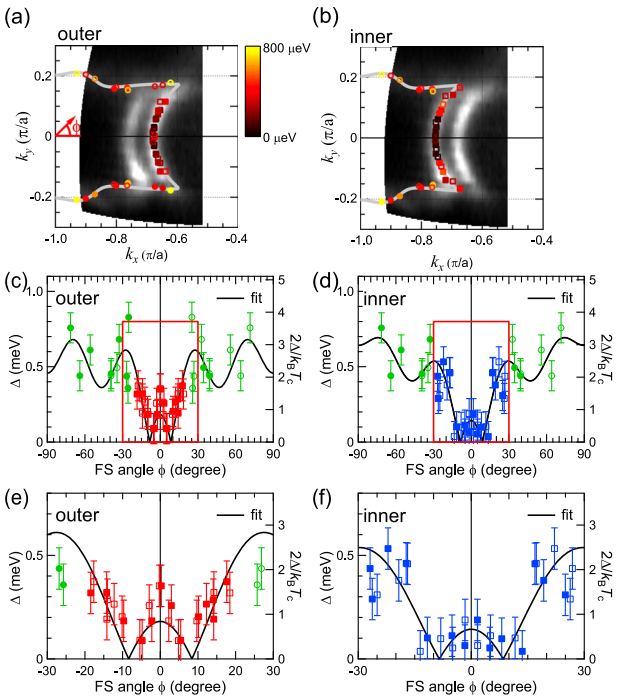

FIG. 3. SC gap anisotropy of $NdO_{0.71}F_{0.29}BiS_2$. (a),(b) The k_F positions at which the SC gap was measured plotted on the FS map image for the outer and inner FSs, respectively. Color scale corresponds to each SC gap size derived from the fitting. Solid symbols are derived from the EDCs shown in Fig. 2; open symbols are plotted after symmetrization, taking into account the tetragonal crystal symmetry. (c),(d) SC gap sizes derived from the fitting plotted as a function of FS angle for the outer and inner FSs, respectively. Error bar denotes the standard deviation of the E_F position (see Supplemental Material and Fig. S6 therein [28]). Solid lines are fitting functions using a model gap function of $\Delta(\phi) = |\Delta_0[1 + \Delta_2\cos(2\phi) + \Delta_4\cos(4\phi) + \Delta_6\cos(6\phi) + \Delta_8\cos(8\phi)]|$. (e),(f) Enlarged plots for the regions indicated by solid squares in (c) and (d), respectively.

the reduced gap size $2\Delta(0)/k_BT_c = 3.76$. One can confirm that the temperature dependence of the deduced SC gap size is in good accordance with that of the BCS theory. Figures 2(c)–2(e) show the symmetrized EDCs at k_F in the degenerate region and the clearly separated regions of the outer and inner FSs, respectively, measured at 1.5 K (below T_c) and 8 K (above T_c). Each symmetrized EDC at k_F is identified with a FS angle ϕ for each FS [Fig. 1(c)]. The valley structures at E_F observed in the symmetrized EDCs of both FSs [Figs. 2(c)–2(e)] indicate the opening of the SC gap, and the flat structure indicates that the SC gap is quite small. For both FSs, the line shape of the symmetrized EDCs at k_F depends strongly on the FS angle, indicating that the SC gap is highly anisotropic.

The SC gap anisotropy deduced from the fitting is shown in Fig. 3. The right axes of Figs. 3(c) and 3(d) correspond to $2\Delta/k_BT_c$, and its maximum is comparable to the BCS value of 3.53. This suggests that our results are reliable but is in contrast to previous reports [13,14]. The open symbols are plotted after symmetrization, taking into account the tetragonal crystal symmetry. Around $\phi = 5°$ for the outer FS and $\phi = 8°$ for the inner FS, Δ shows a cusplike minimum, whereas it is clearly finite at $|\phi| > 15°$. This is also clear from the symmetrized EDCs (see also Fig. S5 of the Supplemental Material [28]). They show flat structures around $\phi = 5°$ for the outer FS and $\phi = 8°$ for the inner FS, whereas they clearly show valley structures at E_F at $|\phi| > 15°$. This indicates the existence of SC gap nodes. Considering the tetragonal crystal symmetry, the FSs around the X point have twofold rotational symmetry, and their SC gap anisotropy should also have twofold symmetry with respect to the X point. Hence, we can use the following function to fit the SC gap anisotropy:

$$\Delta(\phi) = |\Delta_0[1 + \Delta_2\cos(2\phi) + \Delta_4\cos(4\phi) + \Delta_6\cos(6\phi) + \Delta_8\cos(8\phi)]|, \quad (1)$$

for each FS. Although fairly high-order terms are needed for the fitting because the FSs are rectangular rather than ellipsoidal, this fitting function successfully reproduces the SC gap anisotropy of both FSs, as shown in Fig. 3.

Here, we focus on the SC gap anisotropy and origin of the pairing interactions. As shown in Fig. 3, the SC gaps of the outer and inner FSs show strong anisotropies, and we determined that they have nodelike minima. According to

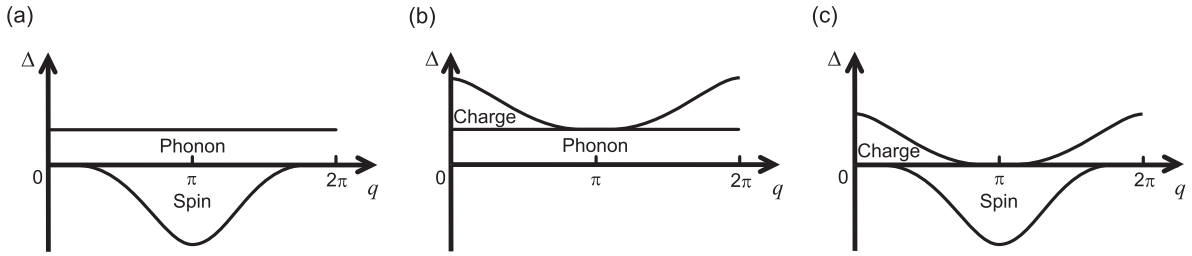

FIG. 4. Schematic illustration of multiple pairing interactions. Positive and negative SC gaps Δ correspond to those originated from attractive and repulsive interactions, respectively. (a) Competition of q-independent conventional electron-phonon coupling and q-dependent repulsive spin fluctuations. (b) Cooperation of q-independent electron-phonon coupling and q-dependent attractive charge fluctuations. (c) Competition of q-dependent attractive charge fluctuations and q-dependent repulsive spin fluctuations. The attractive charge fluctuations are assumed to be peaked at $q = (0, 0)$, whereas the repulsive spin fluctuations are assumed to be peaked at $q = (\pi, \pi)$.

random phase approximation calculations, a similar FS topology can produce a d- or g-wave SC gap symmetry and, hence, a nodal SC gap anisotropy, and its anisotropy is similar to our results that the nodes are located at the short edge of the rectangular FSs [10,18,35]. On the other hand, magnetic penetration depth measurements and thermal transport measurements have indicated nodeless superconductivity in $NdO_{1-x}F_xBiS_2$ ($x = 0.3$ and 0.5) [36,37]. These results may seem to be inconsistent with our results. However, if the SC gap symmetry of $NdO_{1-x}F_xBiS_2$ is s wave and the SC gap nodes are accidental ones, the nodes can be lifted by disorder effects because they are not symmetry protected in nodal s-wave superconductivity. Such a disorder-induced topological change of the SC gap structure from a nodal s wave to a nodeless s wave has been reported for iron-pnictide superconductors [38–40]. For $NdO_{1-x}F_xBiS_2$, the existence of bismuth and sulfur defects has been reported from several experiments [20,21,41], and this could also change the SC gap structure from the nodal s wave to the nodeless one in bulk measurements. On the other hand, ARPES is a surface-sensitive technique, although laser ARPES using a VUV laser is relatively bulk sensitive, and the VUV laser can be focused to a spot size of ~100 μm at the cleaved sample surface by carefully adjusting the focal point of the laser. With this surface sensitivity and small spot size, laser ARPES can probe a region of few defects and detect the highly anisotropic and possibly nodal SC gap structure [42]. In this work, without careful adjustment of the focal point of the laser, we observed an anisotropic but nodeless SC gap, and the sufficiently reproduced data could not be obtained. Because the SC gap anisotropy measured by ARPES is generally suppressed due to the existence of impurities and/or disorders [45], the observed anisotropy should reflect the region free from defects and/or disorders. In addition, if the observed anisotropy is originated from defects and/or disorders, such anisotropy cannot be reproduced because defects and/or disorder should be different for piece-by-piece or sample positions, and, hence, the obtained reproducibility assures that the observed anisotropy is intrinsic.

As mentioned above, our results revealed a strong SC gap anisotropy and suggested the existence of accidental nodes in nodal s-wave symmetry. This should indicate competition or cooperation among multiple pairing interactions. First, a strong SC gap anisotropy suggests contributions from unconventional SC pairing interactions that have a strong q dependence. On the other hand, a finite q-independent component Δ_0 can be expected to originate from the conventional pairing interaction of phonons. Thus, we assumed competition and cooperation among three types of SC pairing interactions as the typical possible origins of superconductivity in $NdO_{0.71}F_{0.29}BiS_2$: (i) q-independent electron-phonon coupling, which produces conventional superconductivity, (ii) q-dependent repulsive spin fluctuations, and (iii) q-dependent attractive charge fluctuations. As schematically shown in Fig. 4, we considered competition and cooperation among these three interactions as the origin of the SC gap anisotropy in $NdO_{0.71}F_{0.29}BiS_2$. Here, positive and negative SC gaps Δ correspond to those originated from attractive and repulsive interactions, respectively. In Fig. 4(a), q-independent electron-phonon coupling and q-dependent spin fluctuations are assumed. Whereas electron-phonon coupling is an attractive interaction, spin fluctuations are originated from a repulsive Coulomb interaction; thus, these interactions should be competitive. In this case, depending on the ratio of these contributions, the SC gap can be nodal. On the other hand, in Fig. 4(b), q-independent electron-phonon coupling and q-dependent attractive charge fluctuations are assumed. In this case, the two interactions are cooperative; thus, the SC gap can be strongly anisotropic but nodeless. In Fig. 4(c), q-dependent repulsive spin fluctuations and attractive charge fluctuations are assumed. Both interactions are anisotropic and the SC gap likely becomes nodal. We cannot conclude which case is the most appropriate for $NdO_{0.71}F_{0.29}BiS_2$, but in any case, it is strongly suggested that the mechanism of superconductivity in $NdO_{0.71}F_{0.29}BiS_2$ is unconventional.

In summary, we investigated the band structure and SC gap anisotropy of $NdO_{0.71}F_{0.29}BiS_2$ by ARPES measurements using a He discharge lamp and a VUV laser.

We observed two electron FSs and found that their SC gaps are strongly anisotropic and have nodelike minima. Whereas the observed SC gap anisotropy is similar to that of the theoretical results, suggesting the possibility of a d or g wave for the SC gap symmetry of $NdO_{0.71}F_{0.29}BiS_2$, an s wave with accidental nodes is strongly suggested from the comparison to the other experimental results. We considered competition and cooperation of multiple pairing interactions and concluded that $NdO_{0.71}F_{0.29}BiS_2$ is an unconventional superconductor.

We thank R. Arita, K. Kuroki, H. Usui, K. Suzuki, and T. Hotta for valuable discussions and comments. This work was supported by the Photon and Quantum Basic Research Coordinated Development Program of MEXT and partially supported by JSPS KAKENHI Grants No. JP25220707 and No. JP26610095.

*Author to whom correspondence should be addressed. okazaki@issp.u-tokyo.ac.jp

†Author to whom correspondence should be addressed. shin@issp.u-tokyo.ac.jp

[1] Y. Mizuguchi, S. Demura, K. Deguchi, Y. Takano, H. Fujihisa, Y. Gotoh, H. Izawa, and O. Miura, J. Phys. Soc. Jpn. **81**, 114725 (2012).

[2] Y. Mizuguchi, H. Fujihisa, Y. Gotoh, K. Suzuki, H. Usui, K. Kuroki, S. Demura, Y. Takano, H. Izawa, and O. Miura, Phys. Rev. B **86**, 220510 (2012).

[3] J. Xing, S. Li, X. Ding, H. Yang, and H.-H. Wen, Phys. Rev. B **86**, 214518 (2012).

[4] S. Demura, Y. Mizuguchi, K. Deguchi, H. Okazaki, H. Hara, T. Watanabe, S. J. Denholme, M. Fujioka, T. Ozaki, H. Fujihisa, Y. Gotoh, O. Miura, T. Yamaguchi, H. Takeya, and Y. Takano, J. Phys. Soc. Jpn. **82**, 033708 (2013).

[5] T. Yildirim, Phys. Rev. B **87**, 020506 (2013).

[6] H. Sakai, D. Kotajima, K. Saito, H. Wadati, Y. Wakisaka, M. Mizumaki, K. Nitta, Y. Tokura, and S. Ishiwata, J. Phys. Soc. Jpn. **83**, 014709 (2014).

[7] J. G. Bednorz and K. A. Müller, Z. Phys. B **64**, 189 (1986).

[8] Y. Kamihara, T. Watanabe, M. Hirano, and H. Hosono, J. Am. Chem. Soc. **130**, 3296 (2008).

[9] Y. Mizuguchi, J. Phys. Chem. Solids **84**, 34 (2015).

[10] H. Usui, K. Suzuki, and K. Kuroki, Phys. Rev. B **86**, 220501 (2012).

[11] J. Lee, M. B. Stone, A. Huq, T. Yildirim, G. Ehlers, Y. Mizuguchi, O. Miura, Y. Takano, K. Deguchi, S. Demura *et al.*, Phys. Rev. B **87**, 205134 (2013).

[12] A. Athauda, J. Yang, S. Lee, Y. Mizuguchi, K. Deguchi, Y. Takano, O. Miura, and D. Louca, Phys. Rev. B **91**, 144112 (2015).

[13] S. Li, H. Yang, D. Fang, Z. Wang, J. Tao, X. Ding, and H. Wen, Sci. China Phys. Mech. Astron. **56**, 2019 (2013).

[14] B. Liu and S. Feng, Europhys. Lett. **106**, 17003 (2014).

[15] G. B. Martins, A. Moreo, and E. Dagotto, Phys. Rev. B **87**, 081102 (2013).

[16] Y. Yang, W.-S. Wang, Y.-Y. Xiang, Z.-Z. Li, and Q.-H. Wang, Phys. Rev. B **88**, 094519 (2013).

[17] C.-L. Dai, Y. Yang, W.-S. Wang, and Q.-H. Wang, Phys. Rev. B **91**, 024512 (2015).

[18] T. Agatsuma and T. Hotta, J, Magn. Magn. Mater. **400**, 73 (2016).

[19] T. Shimojima, K. Okazaki, and S. Shin, J. Phys. Soc. Jpn. **84**, 072001 (2015).

[20] Z. R. Ye, H. F. Yang, D. W. Shen, J. Jiang, X. H. Niu, D. L. Feng, Y. P. Du, X. G. Wan, J. Z. Liu, X. Y. Zhu, H. H. Wen, and M. H. Jiang, Phys. Rev. B **90**, 045116 (2014).

[21] L. K. Zeng, X. B. Wang, J. Ma, P. Richard, S. M. Nie, H. M. Weng, N. L. Wang, Z. Wang, T. Qian, and H. Ding, Phys. Rev. B **90**, 054512 (2014).

[22] M. Nagao, S. Demura, K. Deguchi, A. Miura, S. Watauchi, T. Takei, Y. Takano, N. Kumada, and I. Tanaka, J. Phys. Soc. Jpn. **82**, 113701 (2013).

[23] K. Okazaki, Y. Ota, Y. Kotani, W. Malaeb, Y. Ishida, T. Shimojima, T. Kiss, S. Watanabe, C.-T. Chen, K. Kihou *et al.*, Science **337**, 1314 (2012).

[24] K. Okazaki, Physica C **494**, 54 (2013).

[25] Y. Ota, K. Okazaki, Y. Kotani, T. Shimojima, W. Malaeb, S. Watanabe, C.-T. Chen, K. Kihou, C. H. Lee, A. Iyo *et al.*, Phys. Rev. B **89**, 081103 (2014).

[26] The separation of the two FSs has already been discussed in Ref. [21], and it is consistent with the band-structure calculation, although the separation was not so clearly observed. Here, whereas the separation is not clear for the He-lamp ARPES as in the previous studies, it could be clearly observed for the laser ARPES. This is probably due to the high energy and momentum resolutions, bulk sensitivity, and a small spot size for the laser ARPES measurements.

[27] EDCs before symmetrization and the fitting results are shown in Fig. S2 of the Supplemental Material [28].

[28] See Supplemental Material at http://link.aps.org/supplemental/10.1103/PhysRevLett.118.167002, which includes Refs. [29–34], for additional data analyses.

[29] T. Yokoya, T. Nakamura, T. Matsushita, T. Muro, Y. Takano, M. Nagao, T. Takenouchi, H. Kawarada, and T. Oguchi, Nature (London) **438**, 647 (2005).

[30] K. Hashimoto, K. Cho, T. Shibauchi, S. Kasahara, Y. Mizukami, R. Katsumata, Y. Tsuruhara, T. Terashima, H. Ikeda, M. A. Tanatar, H. Kitano, N. Salovich, R. W. Giannetta, P. Walmsley, A. Carrington, R. Prozorov, and Y. Matsuda, Science **336**, 1554 (2012).

[31] Y. Zhang, Z. R. Ye, Q. Q. Ge, F. Chen, J. Jiang, M. Xu, B. P. Xie, and D. L. Feng, Nat. Phys. **8**, 371 (2012).

[32] T. Shimojima *et al.*, Phys. Rev. B **89**, 045101 (2014).

[33] Iron pnictides have multiple bands, and generally multiple peaks are overlapped in their MDCs. However, by using linearly polarized light and photoemission selection rules, a single band can be selected and its MDC width can be evaluated.

[34] T. Shimojima, F. Sakaguchi, K. Ishizaka, Y. Ishida, T. Kiss, M. Okawa, T. Togashi, C.-T. Chen, S. Watanabe, M. Arita, K. Shimada, H. Namatame, M. Taniguchi, K. Ohgushi, S. Kasahara, T. Terashima, T. Shibauchi, Y. Matsuda, A. Chainani, and S. Shin, Science **332**, 564 (2011).

[35] X. Wu, J. Yuan, Y. Liang, H. Fan, and J. Hu, Europhys. Lett. **108**, 27006 (2014).

[36] L. Jiao, Z. Weng, J. Liu, J. Zhang, G. Pang, C. Guo, F. Gao, X. Zhu, H.-H. Wen, and H. Q. Yuan, J. Phys. Condens. Matter **27**, 225701 (2015).

[37] T. Yamashita, Y. Tokiwa, D. Terazawa, M. Nagao, S. Watauchi, I. Tanaka, T. Terashima, and Y. Matsuda, J. Phys. Soc. Jpn. **85**, 073707 (2016).

[38] V. Mishra, G. R. Boyd, S. Graser, T. Maier, P. J. Hirschfeld, and D. J. Scalapino, Phys. Rev. B **79**, 094512 (2009).

[39] Y. Wang, A. Kreisel, P. J. Hirschfeld, and V. Mishra, Phys. Rev. B **87**, 094504 (2013).

[40] Y. Mizukami, M. Konczykowski, Y. Kawamoto, S. Kurata, S. Kasahara, K. Hashimoto, V. Mishra, A. Kreisel, Y. Wang, P. J. Hirschfeld *et al.*, Nat. Commun. **5**, 5657 (2014).

[41] T. Machida, Y. Fujisawa, M. Nagao, S. Demura, K. Deguchi, Y. Mizuguchi, Y. Takano, and H. Sakata, J. Phys. Soc. Jpn. **83**, 113701 (2014).

[42] Submillimeter-size electronic phase distributions have been reported for cuprates [43] and iron-based superconductors [44], and, thus, disorder and/or defects also could be in this scale.

[43] M. Fratini, N. Poccia, A. Ricci, G. Campi, M. Burghammer, G. Aeppli, and A. Bianconi, Nature (London) **466**, 841 (2010).

[44] A. Ricci, N. Poccia, G. Campi, B. Joseph, G. Arrighetti, L. Barba, M. Reynolds, M. Burghammer, H. Takeya, Y. Mizuguchi, Y. Takano, M. Colapietro, N. L. Saini, and A. Bianconi, Phys. Rev. B **84**, 060511 (2011).

[45] K. Okazaki, Y. Ito, Y. Ota, Y. Kotani, T. Shimojima, T. Kiss, S. Watanabe, C. T. Chen, S. Niitaka, T. Hanaguri, H. Takagi, A. Chainani, and S. Shin, Phys. Rev. Lett. **109**, 237011 (2012).